Phase-Sensitive Sum Frequency Revealing Accommodation of Bicarbonate Ions, and Charge Separation of Sodium and Carbonate Ions within the Air/Water Interface

Wei Hua, Xiangke Chen, and Heather C. Allen*

Department of Chemistry, The Ohio State University, 100 West 18th Avenue, Columbus, Ohio 43210, United States

ABSTRACT: Interfacial water structure plays a key role in many chemical, biological, and environmental processes. Here, in addition to conventional VSFG, we employ phase-sensitive sum frequency generation (PS-SFG) to investigate the average direction of the transition dipole of interfacial water molecules that is intrinsically contained in the sign of the second-order nonlinear susceptibility, $\chi^{(2)}$. The orientation of water at air/aqueous inorganic salt interfaces of Na_2CO_3 and $NaHCO_3$ was

inferred from the direct measurement of the transition dipole moment of the interfacial water molecules. It is found that bicarbonate and its counterion sodium do not significantly perturb the interfacial water structure, whereas carbonate strongly orients water so that the water hydrogens point down toward the bulk solution. This is consistent with the picture of carbonate anions residing many layers below the water surface with a preference for the sodium cations to be above the anions and thereby closer to the topmost layer of the water surface.
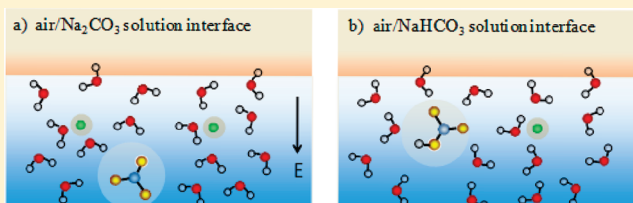
INTRODUCTION

Understanding interfacial water structure of ubiquitous air/aqueous interfaces at the molecular level is of prime importance in environmental chemistry and atmospheric aerosol science.[1,2] The orientations and hydrogen bonding arrangements of water molecules may influence the surface properties and, hence, surface processes and surface reactivity of these systems. Many studies have revealed that it is the properties of the interfacial region that drive the heterogeneous chemistry of atmospheric aerosols.[2−4]

Knowledge of water structure at air/aqueous salt solution interfaces may shed light on reaction mechanisms and gas uptake at aqueous interfaces of environmental interest. For instance, it has been proposed that the presence of water, specifically in the interfacial region, plays an important role in the heterogeneous hydrolysis of ions in the atmosphere.[5] This is particularly relevant to the uptake and the chemical transformation of atmospheric carbon dioxide by atmospheric aerosol and ocean surfaces[6,7] since CO_2 readily undergoes hydration and chemical reaction when in the presence of water.[8−11] For ocean−air interactions, it is the surface aqueous layers that first encounter atmospheric CO_2 prior to and during its transformation to bicarbonate and carbonate.[12]

Currently, ~30% of the CO_2,[6] $1.5 \pm 0.4 \times 10^{14}$ mol, emitted to the atmosphere by human activities is absorbed annually by the ocean. This serves as the largest sustained sink of excess atmospheric CO_2 resulting from fossil fuel burning and results in total inorganic carbon (T_{CO_2}) content of the seawater of ~2000 μmol kg^{-1}.[13] Considering the increasing concentration of CO_2 in the atmosphere (~385 ppm, IPCC 2007)[6] and its potential impact on aqueous surface chemistry in the earth's

hydrological cycle via enhancing acidity of aqueous surfaces, the behavior of carbonate and bicarbonate ions in the interfacial region from reaction of CO_2 with water may be important.[3,14]

Although the flux of CO_2 between the ocean and the atmosphere is influenced by many factors, inclusive of atmospheric concentration (partial pressure), temperature, salinity, and alkalinity, the knowledge of the surface preference and interfacial average location of carbonate and bicarbonate ions at the air/aqueous interface might facilitate a better understanding of the process of CO_2 absorption into the ocean. Moreover, due to decreasing pH of the ocean from increasing atmospheric CO_2 concentrations, the ratio of HCO_3^- to CO_3^{2-} is changing,[6] which then may alter the water organization at the air/ocean interface and air/atmospheric aerosol interfaces, as is suggested from the results presented here. These findings may also be relevant to thundercloud electrification. For example, in atmospheric lightening production, sulfate ions in the surface layer of ice particles are suggested to be responsible for charge transfer in thundercloud electrification,[15] and yet to our knowledge, carbonate and bicarbonate have not been implicated in any part of this process.

To understand the organization of relevant air/aqueous interfaces, we report the interfacial water transition dipole orientation in the presence of Na_2CO_3 and $NaHCO_3$. The location of the solvated ions relative to their respective aqueous

surfaces is inferred using phase-sensitive sum frequency generation (PS-SFG), a variant of vibrational sum frequency generation (VSFG). Additional insight is given on the perturbation of the interfacial water structure for each aqueous salt system.

The seminal publication of the water surface VSFG spectrum was reported in 1993,[17] just two years after the first published account of surface VSFG.[24] SFG is a second-order nonlinear optical process that demonstrates interface specificity and molecular sensitivity. The SFG response vanishes in centrosymmetric media[16] and is sensitive to orientation and ordering of interfacial species.[17−23] VSFG has been applied extensively to characterize air/aqueous interfaces of acidic, basic, and aqueous salt solutions;[20,22,25,26] however, the understanding of how various types of ions alter the interfacial hydrogen-bonding network at the air/water interface—namely, the net water dipole orientation of water molecules at the air/aqueous salt solution—is still quite limited.

Conventional VSFG spectroscopy employs homodyne detection, and its intensity spectrum is proportional to the absolute square of the second-order nonlinear susceptibility, $|\chi^{(2)}|^2$, as shown in eq 1, where I_{SFG}, I_{vis}, and I_{IR} are the intensities of the output SFG, incident visible, and infrared beams, respectively, and $\chi_{NR}^{(2)}$ and $\chi_\nu^{(2)}$ are the nonresonant and resonant second-order nonlinear susceptibilities, respectively.

$$I_{SFG} \propto \left|\chi^{(2)}\right|^2 I_{vis}I_{IR} \propto \left|\chi_{NR}^{(2)} + \sum_\nu \chi_\nu^{(2)}\right|^2 I_{vis}I_{IR} \quad (1)$$

The sign of the complex second-order nonlinear susceptibility, $\chi^{(2)}$, inherently contains the orientation information. Whether the net interfacial water dipole is pointing up toward the vapor side or down toward the bulk water interior is shown in eqs 2 and 3, where A_ν is the transition moment strength, ω_{IR} is the incident infrared frequency, ω_ν is the frequency of the vibrational transition, and Γ_ν is the line width (half width at half-maximum) of the vibrational transition.

$$\chi_\nu^{(2)} = \frac{A_\nu}{\omega_{IR} - \omega_\nu + i\Gamma_\nu} \quad (2)$$

$$\mathrm{Im}\,\chi^{(2)} = -\sum_\nu \frac{A_\nu\Gamma_\nu}{(\omega_{IR} - \omega_\nu)^2 + \Gamma_\nu^2} \quad (3)$$

The conventional VSFG spectrum does not differentiate the net water dipole direction and suffers spectral distortion arising from cross terms that include contributions from the resonant real part of $\chi^{(2)}$ (Re $\chi^{(2)}$), the imaginary part of $\chi^{(2)}$ (Im $\chi^{(2)}$), and the nonresonant term, $\chi_{NR}^{(2)}$. To deduce orientation information from the measured $|\chi^{(2)}|^2$ spectra (i.e., conventional VSFG spectra) in the O−H stretch region, discrete resonances have been assumed by different groups to fit the spectrum.[27,28] However, the overall spectral shape arises from a continuous band of OH stretch resonances of interfacial water molecules that are hydrogen-bonded to neighbors with a wide variety of geometries and strengths.[29,30] Without knowledge of the resonant frequencies and their respective signs of their amplitudes, fitting these spectra becomes somewhat arbitrary. In addition, coupling between water modes also plays a role in the spectral shape. As a result, despite the similarity of VSFG spectra obtained by different groups, detailed interpretation of the spectra often varies.[31,32] This issue is somewhat remedied by using a phase-sensitive SFG method that enables absolute determination of the sign of $\chi^{(2)}$.

PS-SFG has been pioneered by Shen and co-workers.[29,30,33−35] Benderskii and co-workers,[36] and Tahara and co-workers[37,38] developed this technique for broad-bandwidth VSFG systems. The PS-SFG method is based on interference of the sample response with an additional signal of phase reference and, hence, provides the imaginary part of the nonlinear susceptibility $\chi^{(2)}$, Im $\chi^{(2)}$, which directly reveals the net water dipole orientation of surface species. In the current literature, PS-SFG has been utilized to elucidate the interfacial hydrogen-bonding network at air/neat water (including isotopic dilution by D_2O), air/acid or basic solution, air/lipid, and air/surfactant interfaces.[29,30,33−35,37,38]

■ EXPERIMENTAL SECTION

Materials and Preparation of Salts Solutions. Sodium carbonate (99.5−100.5%) was obtained from Mallinckrodt chemicals. Sodium bicarbonate (powder/certified ACS) was purchased from Fisher Scientific. The sodium carbonate salt was heated at 650 °C for 10 h before dissolving in Nanopure water. Nanopure water (not purged of CO_2) with a resistivity of 18.2−18.3 MΩ·cm and a measured pH of 5.5 was from a Barnstead Nanopure system (model D4741) with additional organic removing cartridges (D5026 Type I ORGANICfree Cartridge Kit; Pretreat Feed).

Stock solutions were prepared by dissolving salts in Nanopure water and then were filtered using a Whatman Carbon-Cap activated carbon filter, typically three times to eliminate organic impurities. Raman spectra were utilized to generate a calibration curve, and the concentrations of stock solutions were determined from the calibration curve. To facilitate comparison with previous conventional SFG studies and MD simulations,[39,40] 0.8 and 1.1 M salt solutions were chosen in this study and then prepared by dilutions of desired amounts of stock solutions. The measured pH of 1.1 M Na_2CO_3 and 0.8 M $NaHCO_3$ solutions were 11.7 and 8.8, respectively. The resultant concentration of OH^- ions in the 1.1 M Na_2CO_3 was 0.005 M, relatively small compared with the salt ions. Owing to the sensitivity of SFG spectroscopy to organic contamination, all of the water and salt solutions were proved to be free of organic impurities as revealed by the VSFG spectra obtained in the C−H region of 2800 to 3000 cm^{-1}. In addition, all solutions were conditioned at room temperature (23 ± 1 °C) over 24 h before use.

Methods: Phase-Sensitive Sum Frequency Generation (PS-SFG). The broad-bandwidth VSFG spectrometer setup has been described elsewhere,[26,41−43] with the PS-SFG setup briefly described more recently.[44,45] For the visible and infrared light generation, a titanium:sapphire oscillator (792 nm)/double regenerative amplifier system (1 kHz) (Spectra-Physics) was used. The amplifiers generate ~85 fs pulses at 792 nm (22 nm bandwidth, >1 W) and 2 ps pulses at 792 nm (17 cm^{-1} bandwidth, >500 mW, used as the visible beam). The broadband femtosecond laser pulses (~ 85 fs, >1 W) were used to generate a tunable broadband infrared beam in an optical parametric amplifier (Light Conversion, TOPAS), followed by a nonlinear difference-frequency generation system (Light Conversion, NDFG connected to the TOPAS). The full spectral bandwidth of the generated broadband infrared beam was ~500 cm^{-1} in the region under investigation. The average power of the visible beam and the infrared beam were 300 μJ and 10 μJ, respectively. The visible beam (s-polarized, 792 nm) and the infrared beam

6234

dx.doi.org/10.1021/jp111552f |J. Phys. Chem. A 2011, 115, 6233–6238
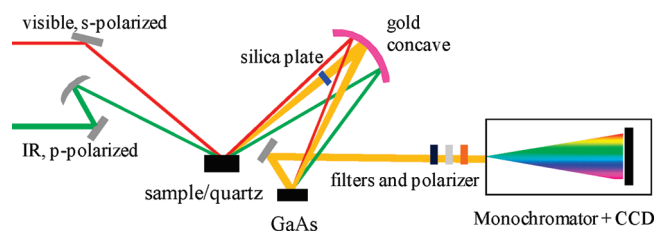
Figure 1. Schematic of the phase-sensitive SFG experiment optical configuration. Filters and polarizer denote two short-pass filters, a notch filter, and a Glan-Thompson polarizer, respectively, from left to right.

(p-polarized, OH stretch region) were spatially and temporally overlapped on the sample stage (for samples and z-cut quartz) with incident angles of 50° and 60°, respectively, to generate the sum frequency beam (s-polarized).

The PS-SFG sample and detection setup used here is similar to the system reported by Tahara and co-workers,[37,38] which is based on heterodyne detection of broad bandwidth signals and Fourier transform analysis. The essential part of optical configuration in our broad bandwidth VSFG system was redesigned for the PS-SFG application, as is shown in Figure 1.[44] Upon reflection from the sample stage, the incident visible, infrared, and generated sum frequency (s-polarized) beams were refocused by a gold concave mirror (f = 100 mm) onto a GaAs (Lambda Precision Optics) surface to generate another sum frequency beam (local oscillator, LO). The sum frequency beam from the sample stage passed through a 1-mm-thick silica plate positioned before the gold concave mirror and was delayed by ~2.6 ps. The two sum frequency beams from different stages with a delay in time domain generated an interference fringe in the frequency domain, and then this interferogram was stretched in a monochromator (Acton Research, SpectraPro SP-500 monochromator with a 1200 g/mm grating blazed at 750 nm) and then detected by a liquid-nitrogen-cooled, charge-coupled device (CCD) (Roper Scientific, 1340 × 400 pixel array, Spec-10:400B: LN400EB back-illuminated CCD). The height of the sample surface that was checked by the image on the CCD is critical for accurate phase determination. Neat water was used as a reference for the pixel height. Height accuracy was better than 10 μm, where each CCD pixel is 20 × 20 μm. Final spectra were processed from the raw interferograms through Fourier transformation and were averaged over the two consecutive runs with 5 min integration times for each sample. The data processing procedure is described in the Supporting Information of a previous publication.[44] PS-SFG spectra are presented from 3000 to 3500 cm^{-1}. Work is under way in our laboratory to further expand our available PS-SFG bandwidth.

■ RESULTS AND DISCUSSION

Air/aqueous solution interfaces of Na_2CO_3 and $NaHCO_3$ salts have been previously investigated by conventional VSFG methods and MD simulation,[39,40] yet no direct PS-SFG measurement has been conducted. Here, we probe the net transition dipole orientation of the interfacial water molecules in the presence of these salts in the OH stretching region. The relative placement of the cations and anions, their average distribution, in the interfacial region is then inferred.

Neat Water. Considering that we use the air/neat water interface as a reference for all spectra, to facilitate the discussion, the PS-SFG spectrum of the air/neat water interface and its
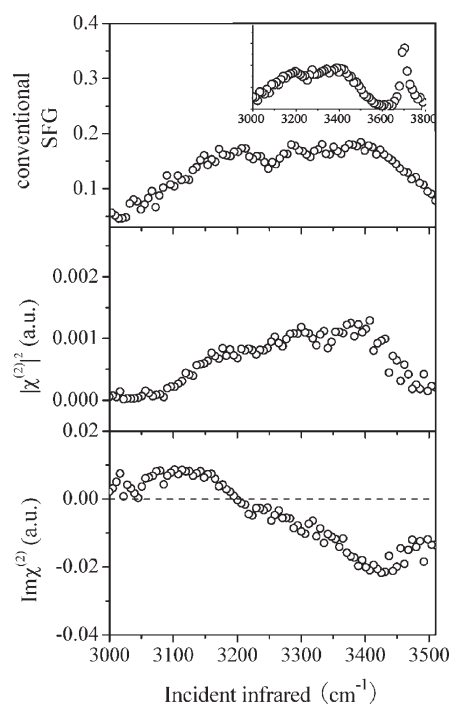
Figure 2. Phase-sensitive and conventional VSFG spectra of neat water: Im $\chi^{(2)}$ SFG spectra (bottom panel), deduced power spectrum (middle panel), conventional VSFG spectra (top panel). The inset in the top panel is a full conventional VSFG spectrum from 3000 to 3800 cm^{-1}.

spectral interpretation is presented. To check the validity of the spectra, the deduced power $|\chi^{(2)}|^2$ spectrum of neat water from PS-SFG with that measured directly from the conventional VSFG setup is compared. In this work, we focus on the hydrogen bonding region as discussed above; in the inset of Figure 2, the spectral range is expanded for the conventional VSFG to include the dangling (free) OH region for reference. As determined by others and clearly accepted by researchers in this field, the dangling OH oscillator points into the air phase.[17,29,30,37] In Figure 2 (top and middle panels), the conventional VSFG and the deduced $|\chi^{(2)}|^2$ spectra are shown and are observed to be similar, although the lowest and highest frequency edges of the deduced $|\chi^{(2)}|^2$ spectrum are lower in SFG intensity. This is due to low incident infrared energy (because of partitioning to the LO) of the spectral edges of the PS-SFG setup. Most obvious in the deduced $|\chi^{(2)}|^2$ spectrum is the relatively low SFG intensity from 3000 to 3100 cm^{-1}. In this case, the incident infrared energy is insufficient to adequately pump the transitions, and normalization procedures do not remedy the problem.

As mentioned above, the Im $\chi^{(2)}$ spectra directly provide informative details, the sign, and thus, transition dipole orientation of each mode in addition to resonance information. The Im $\chi^{(2)}$ spectrum of neat water in the hydrogen-bonded stretching region presented here (Figure 2 bottom panel) is similar to the results reported by Shen and co-workers and Tahara and co-workers.[29,30,37] As revealed in Figure 2, the sign of Im $\chi^{(2)}$ is positive in the region from 3000 to 3200 cm^{-1} and mostly represents the OH stretches in this subspectral region with a net orientation pointing up toward the vapor side of the interface. Recent theoretical investigations by Morita and co-workers[46,47] bring into question the assignment of absolute orientation from the 3000−3200 cm^{-1} region, yet we can confidently assign the
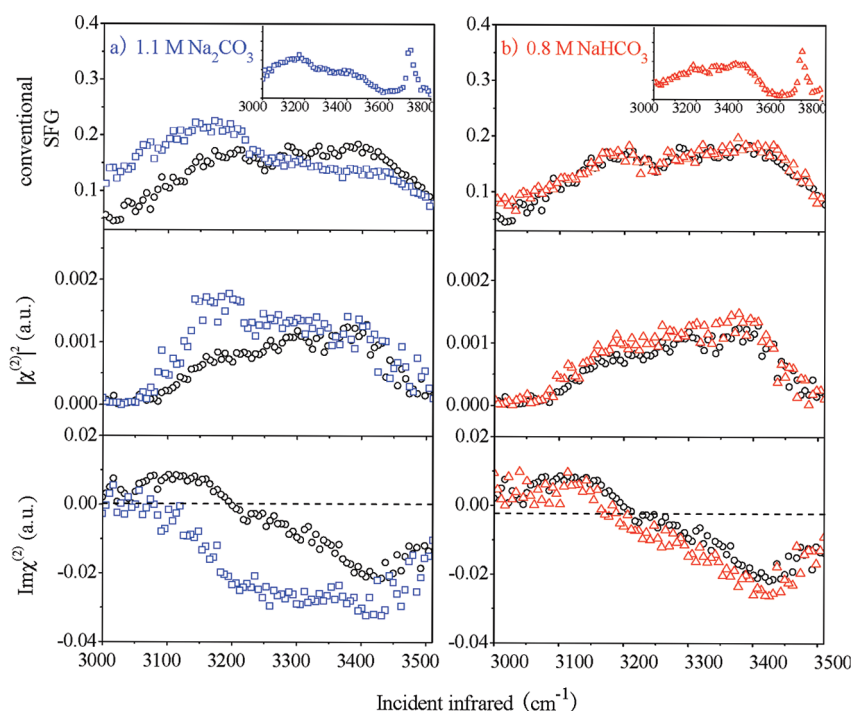
Figure 3. Phase-sensitive and conventional VSFG spectra of water molecules at different vapor/aqueous salts solution interfaces: (a) 1.1 M Na_2CO_3, (b) 0.8 M $NaHCO_3$ salt solution. Im $\chi^{(2)}$ SFG spectra (bottom panel), deduced power spectrum (middle panel), conventional VSFG spectra (top panel). Water spectra are shown as a reference (black circles). The insets in the top panels are conventional VSFG spectra showing the full $3000-3800$ cm^{-1} region.

absolute transition dipole orientation of water molecules for those molecules that contribute to the more weakly hydrogen-bonded spectral region; that is, from 3200 to 3500 cm^{-1}. This spectral region encompasses a large fraction of the SFG intensity and bandwidth. The Im $\chi^{(2)}$ spectrum reveals a negative band above 3200 cm^{-1}, indicating that water molecules have a net transition dipole orientation with their hydrogens pointing down toward the bulk, although it is likely that the distribution of orientations is broad. It was also suggested by others that the top few layers of the water surface are largely responsible for the observed SF spectra and the subsequent layers make little contribution due to the rapid decay of interfacial molecular ordering when approaching isotropic bulk.[29,30,37]

The salt solution SFG spectra are shown in Figure 3. For comparison, the conventional VSFG, deduced $|\chi^{(2)}|^2$, and the Im $\chi^{(2)}$ spectra are shown for the air/liquid interface of neat water (taken from Figure 2), 1.1 M Na_2CO_3, and 0.8 M $NaHCO_3$.

Na_2CO_3. We first consider the aqueous Na_2CO_3 solution. In the left column, the conventional VSFG, deduced $|\chi^{(2)}|^2$, and the Im $\chi^{(2)}$ spectra are shown. The Na_2CO_3 conventional VSFG spectra are in good agreement with conventional spectra obtained by Richmond et al..[40] The overall shape of the hydrogen-bonded OH stretching region of the directly measured conventional VSFG spectrum and the deduced $|\chi^{(2)}|^2$ spectrum is similar, as expected. There is a slightly lower intensity in the low-frequency region of the deduced $|\chi^{(2)}|^2$ spectrum due to the lower energies used in the PS-SFG setup, as was discussed above for the neat water spectra. In addition, the relatively large LO signal enhances the noise in the low-energy wings, and this also cannot be normalized out. However, comparison between the water spectra in the same panel reveals interesting and valid differences.

When comparing the Na_2CO_3 solution spectra with that from neat water, the conventional and deduced $|\chi^{(2)}|^2$ Na_2CO_3 spectrum (top and middle panels) shows an enhanced intensity below 3200 cm^{-1} and a weakened intensity at $\sim$3400 cm^{-1} relative to neat water. This suggests that there is a strengthening of the hydrogen bonds. However, it is evident from the Im $\chi^{(2)}$ spectrum of the air/Na_2CO_3 solution interface that in addition, there are significant changes at and above 3200 cm^{-1} compared with the neat water Im $\chi^{(2)}$ spectrum. The sign of the band below 3200 cm^{-1} flips from positive to negative in the presence of Na_2CO_3 salts, and a significantly stronger negative strength is observed in the Im $\chi^{(2)}$ spectrum from 3200 to 3450 cm^{-1} as compared with the neat water case.

As mentioned, the resultant concentration of OH$^-$ ions in the 1.1 M Na_2CO_3 solution was 0.005 M, relatively small compared with the concentration of the salt ions. In addition, according to Shen and co-workers, in the Im $\chi^{(2)}$ spectrum of the 1.2 M NaOH solution, the intensity of the negative 3400 cm^{-1} band was slightly weaker compared with neat water. We hence propose that the resultant OH$^-$ ions in our Na_2CO_3 solution have a minor impact on the strengthening of the negative band in the Im $\chi^{(2)}$ spectrum.

As stated above, the sign of the Im $\chi^{(2)}$ spectra unambiguously reflects the net polar orientation of the corresponding OH stretches for the spectral region above 3200 cm^{-1}. The negative sign from the spectrum reveals the net dipole orientation of interfacial water molecules with their hydrogen pointing down toward the bulk interior. The strong negative band in the Im $\chi^{(2)}$ spectrum suggests a relatively large fraction of interfacial water molecules have their dipole pointing toward the bulk solution in the presence of Na_2CO_3 salts. We interpret this finding arising from an electric field induced by the organization of near-surface
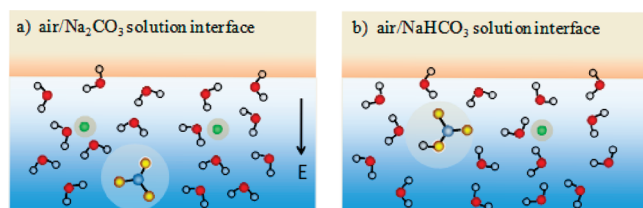
Figure 4. Illustration of water orientation at the air/aqueous salt solution interface of (a) 1.1 M Na_2CO_3 and (b) 0.8 M $NaHCO_3$. Carbon and oxygen in carbonate and bicarbonate ions are bluish-gray and yellow spheres respectively, and sodium ions are green.

sodium ions and near-interior carbonate ions in the aqueous interfacial region.

It has been pointed out that as small and relatively less polarizable ions, sodium cations are repelled from the surface.[35,40,48−50] Hence, it is not likely that sodium ions exist at the very surface, but may exist in the subsurface region (termed near-surface above) to maintain their full hydration. However, on the basis of our data, sodium ions appear to exist above the carbonate ions to provide the necessary field to align the water dipole with hydrogens pointing down (toward the carbonate). Therefore, the PS-SFG result provides experimental evidence suggesting that the counter anions, that is, carbonate ions, are strongly repelled from the surface and reside on the bottom edge of the interfacial region (where lack of inversion symmetry ends), whereas sodium ions reside, on average, above the carbonate ions in the interface, as illustrated in Figure 4a. This result is also supported by MD simulations by Miller and co-workers who proposed the repulsion of carbonate ions from the air/aqueous solution interface.[39]

NaHCO$_3$. In addition to divalent carbonate anions, the interfacial water organization and structure at the air/aqueous interface in the presence of $NaHCO_3$ was investigated. As shown in the column on the right of Figure 3, the conventional, deduced $|\chi^{(2)}|^2$ and the Im $\chi^{(2)}$ SFG spectra from the 0.8 M $NaHCO_3$ solution closely resemble those from neat water. This was somewhat unexpected, although for the conventional VSFG spectrum, the spectrum is consistent with previously published spectra from literature.[39,40]

When comparing the 0.8 M $NaHCO_3$ conventional and deduced $|\chi^{(2)}|^2$ SFG spectra from Figure 3 (top and middle panel), the overall shape of the hydrogen bonding OH region is similar, taking into account the slightly lower intensity in the low-frequency region, as discussed above. When comparing the conventional and deduced $|\chi^{(2)}|^2$ $NaHCO_3$ spectra with those from neat water, there are no notable differences. This is also true for the comparison of the Im $\chi^{(2)}$ SFG spectra from the 0.8 M $NaHCO_3$ relative to neat water. The pH of the 0.8 M $NaHCO_3$ was 8.8; therefore, there is a relatively small concentration ($\sim10^{-5}$ M) of OH^- ions in the solution. We assert that this relatively low OH^- concentration exerts little impact on the Im $\chi^{(2)}$ spectrum. Notably, contrary to the flip of sign of the band at 3200 cm^{-1} observed in the Im $\chi^{(2)}$ spectrum in the presence of Na_2CO_3 salts, no appreciable changes are observed for the 0.8 M $NaHCO_3$ solution, which implies that the net polar orientation and structure of water molecules in the interface is unchanged relative to the air/neat water interface. This also then implies that the bicarbonate and sodium ions are effectively dispersed in the hydrogen bonding network and do not have any appreciable preference for any specific region of the interface, as illustrated in

Figure 4b. The sodium and bicarbonate ions in the 0.8 M $NaHCO_3$ solution do not perturb the interfacial water structure to any appreciable amount and are accommodated in this region. An alternative explanation could be that the ions do not exist in the first several hundred nanometers below the surface; however, this is highly unlikely. (The SFG probe region, if not centrosymmetric, corresponds to roughly half of the shortest incident wavelength.)

On the other hand, it has been reported that $NaHCO_3$ has a negative adsorption, as interpreted from an increase in surface tension relative to neat water, albeit a much more modest increase relative to that determined for sodium carbonate.[51] The relatively smaller effect on surface tension is consistent with the smaller effect on the interfacial water structure as observed here, yet the interpretation of negative adsorption clearly lacks the important details of preferential location of the ions in the interfacial region, as suggested above.

Atmospheric Aerosol and Ocean Surface Chemistry Implications. Aqueous phase aerosols and the ocean's surface absorb atmospheric gas phase CO_2, and given the solubility of CO_2 into water, carbonate concentrations of $1-10$ μM and bicarbonate concentrations of 0.4 to 1.6 mM (calculated temperature range of 0 to 25 °C) currently exist,[13] as calculated for the pH of seawater (7.75 to 8.2).[6] Given the increasing concentration of CO_2 in the atmosphere, interfacial residence and chemistry of atmospheric aerosol and ocean surface water is important in considering the reactivity and uptake by these aqueous surfaces. Here, we have shown that carbonate creates an increase in the interfacial thickness and creates a subsurface field by maintaining a charge separation between sodium and the less-surface-active carbonate, whereas bicarbonate and its countercation sodium intercalate in the dynamic matrix of the hydrogen bonding environment within the first few layers of the water surface. Although beyond the scope of this work, it is likely that the charge separation induced by carbonate will be maintained by sodium and carbonate ions, even in the presence of bicarbonate. This suggests that the surface of aerosol and of the ocean will be impacted by changing ratios of carbonate to bicarbonate as atmospheric CO_2 concentrations continue to increase.

■ CONCLUSIONS

Here, we have shown that CO_3^{2-} anions are buried well below the surface in a 1.1 M Na_2CO_3 aqueous solution, and that the sodium counter cations preferentially reside closer to the surface than the carbonate anions. This was inferred from directly determining that the water molecules in the interfacial region have their hydrogens, on average, pointing down toward the bulk aqueous solution. This preferred orientation arises from charge separation in the interfacial region where, on average, the positively charged sodium cations are above the negatively charged divalent carbonate anions. Future work in our laboratory will focus on quantitatively assessing the anion−cation separation in the interfacial region by carrying out additional PS-SFG studies of this salt at varying concentrations.

The bicarbonate ions organize very differently relative to the carbonate ions. It is inferred that the bicarbonate monovalent anions incorporate into the hydrogen bonding structure of the interfacial water molecules and the sodium cations reside on average near to the same depth as the bicarbonate anions. Thus, water structure is not significantly perturbed with the introduction of 0.8 M $NaHCO_3$. Deciphering how close the bicarbonate

6237

dx.doi.org/10.1021/jp111552f |*J. Phys. Chem. A* 2011, 115, 6233–6238

approaches the surface is still somewhat unclear; however, if only the first few layers of water molecules give rise to the SFG signal intensity for the neat water surface, then bicarbonate and its counter cation sodium likely also reside in this region.

■ AUTHOR INFORMATION

Corresponding Author
*allen@chemistry.ohio-state.edu.

■ ACKNOWLEDGMENT

■ REFERENCES

(1) Jungwirth, P.; Tobias, D. J. *Chem. Rev.* **2006**, *106*, 1259–1281.
(2) Knipping, E. M.; Lakin, M. J.; Foster, K. L.; Jungwirth, P.; Tobias, D. J.; Gerber, R. B.; Dabdub, D.; Finlayson-Pitts, B. J. *Science* **2000**, *288*, 301–306.
(3) Finlayson-Pitts, B. J.; Pitts, J. N., Jr. *Chemistry of the Upper and Lower Atmosphere: Theory, Experiments and Applications*; Academic Press: San Diego, CA, 2000.
(4) Finlayson-Pitts, B. J. *Chem. Rev.* **2003**, *103*, 4801–4822.
(5) Kane, S. M.; Caloz, F.; Leu, M. T. *J. Phys. Chem. A* **2001**, *105*, 6465–6470.
(6) Logan, C. A. *Bioscience* **2010**, *60*, 819–828.
(7) Sabine, C. L.; Feely, R. A.; Gruber, N.; Key, R. M.; Lee, K.; Bullister, J. L.; Wanninkhof, R.; Wong, C. S.; Wallace, D. W. R.; Tilbrook, B.; Millero, F. J.; Peng, T. H.; Kozyr, A.; Ono, T.; Rios, A. F. *Science* **2004**, *305*, 367–371.
(8) Soli, A. L.; Byrne, R. H. *Mar. Chem.* **2002**, *78*, 65–73.
(9) Millero, F. J.; Pierrot, D.; Lee, K.; Wanninkhof, R.; Feely, R.; Sabine, C. L.; Key, R. M.; Takahashi, T. *Deep-Sea Res., Part I* **2002**, *49*, 1705–1723.
(10) Meng, Z. Y.; Seinfeld, J. H.; Saxena, P.; Kim, Y. P. *Aerosol Sci. Technol.* **1995**, *23*, 131–154.
(11) Rudolph, W. W.; Fischer, D.; Irmer, G. *Appl. Spectrosc.* **2006**, *60*, 130–144.
(12) McGillis, W. R.; Edson, J. B.; Zappa, C. J.; Ware, J. D.; McKenna, S. P.; Terray, E. A.; Hare, J. E.; Fairall, C. W.; Drennan, W.; Donelan, M.; DeGrandpre, M. D.; Wanninkhof, R.; Feely, R. A. *J. Geophys. Res., [Oceans]* **2004**, *109*, 1–17.
(13) McGillis, W. R.; Wanninkhof, R. *Mar. Chem.* **2006**, *98*, 100–108.
(14) Buch, V.; Milet, A.; Vacha, R.; Jungwirth, P.; Devlin, J. P. *Proc. Natl. Acad. Sci. U.S.A.* **2007**, *104*, 7342–7347.
(15) Jungwirth, P.; Rosenfeld, D.; Buch, V. *Atmos. Res.* **2005**, *76*, 190–205.
(16) Lambert, A. G.; Davies, P. B. *Appl. Spectrosc. Rev.* **2005**, *40*, 103–145.
(17) Du, Q.; Superfine, R.; Freysz, E.; Shen, Y. R. *Phys. Rev. Lett.* **1993**, *70*, 2313–2316.
(18) Du, Q.; Freysz, E.; Shen, Y. R. *Science* **1994**, *264*, 826–828.
(19) Shultz, M. J.; Schnitzer, C.; Simonelli, D.; Baldelli, S. *Int. Rev. Phys. Chem.* **2000**, *19*, 123–153.
(20) Richmond, G. L. *Chem. Rev.* **2002**, *102*, 2693–2724.
(21) Gopalakrishnan, S.; Liu, D. F.; Allen, H. C.; Kuo, M.; Shultz, M. J. *Chem. Rev.* **2006**, *106*, 1155–1175.
(22) Shen, Y. R.; Ostroverkhov, V. *Chem. Rev.* **2006**, *106*, 1140–1154.
(23) Fan, Y. B.; Chen, X.; Yang, L. J.; Cremer, P. S.; Gao, Y. Q. *J. Phys. Chem. B* **2009**, *113*, 11672–11679.
(24) Superfine, R.; Huang, J. Y.; Shen, Y. R. *Phys. Rev. Lett.* **1991**, *66*, 1066–1069.
(25) Shultz, M. J.; Baldelli, S.; Schnitzer, C.; Simonelle, D. *J. Phys. Chem. B* **2002**, *106*, 5313–5324.

(26) Allen, H. C.; Casillas-Ituarte, N. N.; Sierra-Hernandez, M. R.; Chen, X. K.; Tang, C. Y. *Phys. Chem. Chem. Phys.* **2009**, *11*, 5538–5549.
(27) Liu, D. F.; Ma, G.; Levering, L. M.; Allen, H. C. *J. Phys. Chem. B* **2004**, *108*, 2252–2260.
(28) Raymond, E. A.; Richmond, G. L. *J. Phys. Chem. B* **2004**, *108*, 5051–5059.
(29) Ji, N.; Ostroverkhov, V.; Tian, C. S.; Shen, Y. R. *Phys. Rev. Lett.* **2008**, *100*, 096102–096104.
(30) Tian, C. S.; Ji, N.; Waychunas, G. A.; Shen, Y. R. *J. Am. Chem. Soc.* **2008**, *130*, 13033–13039.
(31) Levering, L. M.; Sierra-Hernandez, M. R.; Allen, H. C. *J. Phys. Chem. C* **2007**, *111*, 8814–8826.
(32) Tarbuck, T. L.; Ota, S. T.; Richmond, G. L. *J. Am. Chem. Soc.* **2006**, *128*, 14519–14527.
(33) Tian, C. S.; Shen, Y. R. *J. Am. Chem. Soc.* **2009**, *131*, 2790–2791.
(34) Tian, C. S.; Shen, Y. R. *Chem. Phys. Lett.* **2009**, *470*, 1–6.
(35) Tian, C. S.; Shen, Y. R. *Proc. Natl. Acad. Sci. U.S.A.* **2009**, *106*, 15148–15153.
(36) Stiopkin, I. V.; Jayathilake, H. D.; Bordenyuk, A. N.; Benderskii, A. V. *J. Am. Chem. Soc.* **2008**, *130*, 2271–2275.
(37) Nihonyanagi, S.; Yamaguchi, S.; Tahara, T. *J. Chem. Phys.* **2009**, *130*, 204704–204708.
(38) Nihonyanagi, S.; Yamaguchi, S.; Tahara, T. *J. Am. Chem. Soc.* **2010**, *132*, 6867–6869.
(39) Du, H.; Liu, J.; Ozdemir, O.; Nguyen, A. V.; Miller, J. D. *J. Colloid Interface Sci.* **2008**, *318*, 271–277.
(40) Tarbuck, T. L.; Richmond, G. L. *J. Am. Chem. Soc.* **2006**, *128*, 3256–3267.
(41) Hommel, E. L.; Ma, G.; Allen, H. C. *Anal. Sci.* **2001**, *17*, 1325–1329.
(42) Ma, G.; Allen, H. C. *J. Phys. Chem. B* **2003**, *107*, 6343–6349.
(43) Tang, C.; Allen, H. J. *J. Phys. Chem. A* **2009**, *113*, 7383–7393.
(44) Chen, X. K.; Hua, W.; Huang, Z. S.; Allen, H. C. *J. Am. Chem. Soc.* **2010**, *132*, 11336–11342.
(45) Chen, X. K.; Allen, H. C. *J. Phys. Chem. B* **2010**, *114*, 14983–14988.
(46) Ishiyama, T.; Morita, A. *J. Phys. Chem. C* **2009**, *113*, 16299–16302.
(47) Ishiyama, T.; Morita, A. *J. Chem. Phys.* **2009**, *131*, 244714–244717.
(48) Gopalakrishnan, S.; Jungwirth, P.; Tobias, D. J.; Allen, H. C. *J. Phys. Chem. B* **2005**, *109*, 8861–8872.
(49) Jungwirth, P.; Tobias, D. J. *J. Phys. Chem. B* **2001**, *105*, 10468–10472.
(50) Mucha, M.; Frigato, T.; Levering, L. M.; Allen, H. C.; Tobias, D. J.; Dang, L. X.; Jungwirth, P. *J. Phys. Chem. B* **2005**, *109*, 7617–7623.
(51) Ozdemir, O.; Karakashev, S. I.; Nguyen, A. V.; Miller, J. D. *Int. J. Miner. Process.* **2006**, *81*, 149–158.

6238

dx.doi.org/10.1021/jp111552f |*J. Phys. Chem. A* 2011, 115, 6233–6238